

## Supporting Information

### Low-Crystalline Bimetallic Metal-Organic Framework Electrocatalysts with Rich Active Sites for Oxygen Evolution

Jiantao Li,<sup>1,‡</sup> Wenzhong Huang,<sup>1,‡</sup> Manman Wang,<sup>1</sup> Shibo Xi,<sup>2</sup> Jiashen Meng,<sup>1</sup> Kangning Zhao,<sup>1</sup> Jun Jin,<sup>3</sup> Wangwang Xu,<sup>4</sup> Zhaoyang Wang,<sup>1</sup> Xiong Liu,<sup>1</sup> Qiang Chen,<sup>1</sup> Linhan Xu,<sup>5</sup> Xiaobin Liao,<sup>1</sup> Yalong Jiang,<sup>1</sup> Kwadwo Asare Owusu,<sup>1</sup> Benli Jiang,<sup>1</sup> Chuanxi Chen,<sup>1</sup> Danian Fan,<sup>1</sup> Liang Zhou<sup>\*,1</sup> and Liqiang Mai<sup>\*,1</sup>

<sup>1</sup>State Key Laboratory of Advanced Technology for Materials Synthesis and Processing, International School of Materials Science and Engineering, Wuhan University of Technology, Wuhan 430070, Hubei, China.

<sup>2</sup>Institute of Chemical and Engineering Sciences, A\*STAR, 1 Pesek Road, Jurong Island 627833, Singapore

<sup>3</sup>School of Chemical and Biomedical Engineering, Nanyang Technological University, 50 Nanyang Avenue, Singapore 639798, Singapore

<sup>4</sup>Department of Mechanical & Industrial Engineering, Louisiana State University, Baton Rouge, USA

<sup>5</sup>Department of Physics and Collaborative Innovation Center for Optoelectronic Semiconductors and Efficient Devices, Xiamen University, Xiamen 361005, Fujian, China

## 1. Experimental Section

### 1.1 Chemicals

All chemicals, including  $\text{Ni}(\text{NO}_3)_2 \cdot 6\text{H}_2\text{O}$  (98%, Sinopharm Chemicals), terephthalic acid (1,4-benzenedicarboxylic acid,  $\text{H}_2\text{BDC}$ ; 99%, aladin),  $\text{FeCl}_3 \cdot 6\text{H}_2\text{O}$  (99%, Sinopharm Chemicals) and  $\text{KOH}$  (98%, Sinopharm Chemicals) were purchased from commercial suppliers and used without further purification.

### 1.2 Synthesis of $\text{Fe}_x\text{Ni}_y\text{-BDC}$ ( $x/y = 1/0, 2/1, 1/1, 1/2, 1/4$ )

In a typical synthesis of  $\text{Fe}_1\text{Ni}_2\text{-BDC}$ ,  $\text{H}_2\text{BDC}$  (1.5 mmol, 0.2492 g),  $\text{FeCl}_3 \cdot 6\text{H}_2\text{O}$  (0.5 mmol, 0.1351 g), and  $\text{Ni}(\text{NO}_3)_2 \cdot 6\text{H}_2\text{O}$  (1.0 mmol, 0.2908 g) were added to 35 mL of dimethyl formamide (DMF) in a Teflon vessel (50 mL) in sequence. The mixture was then stirred 30 minutes to form a uniform solution. The vessel was transferred to a stainless steel autoclave, placed upright in an oven and heated at  $140^\circ\text{C}$  for 4 h before it was cooled to room temperature. The final product was collected by centrifuge, repetitively washed with DMF, anhydrous ethanol, water and lyophilized and freeze dry overnight.

The similar procedure was adopted for the preparation of  $\text{Fe-BDC}$ ,  $\text{Fe}_2\text{Ni}_1\text{-BDC}$ ,  $\text{Fe}_1\text{Ni}_1\text{-BDC}$ ,  $\text{Fe}_1\text{Ni}_2\text{-BDC}$  and  $\text{Fe}_1\text{Ni}_4\text{-BDC}$  except using different molar ratios of  $\text{FeCl}_3 \cdot 6\text{H}_2\text{O}$  and  $\text{Ni}(\text{NO}_3)_2 \cdot 6\text{H}_2\text{O}$  at the beginning (the total mole number of metal ions was kept at 1.5 mmol).

### 1.3 Characterization

X-ray diffraction (XRD) patterns were recorded on a Bruker D8 Discover X-ray diffractometer with  $\text{Cu K}_\alpha$  radiation ( $\lambda = 1.5418 \text{ \AA}$ ). Scanning electron microscopy (SEM, JEOL

JSM-7100F) and transmission electron microscopy (TEM, Titan G2 60-300) were employed to characterize morphologies of the samples. The elemental mapping was collected by the TEM equipped with an energy-dispersive X-ray spectroscope (EDS). X-ray photoelectron spectroscopy (XPS) measurements were performed on a ESCALAB 250Xi system. CHNS/O elemental analyzer was applied to determine the carbon content. The Inductively Coupled Plasma-Optical Emission Spectro (ICP-OES) was employed to analyse the content of Fe/Ni element on Prodigy 7. Fourier transform infrared (FT-IR) spectra were tested on Nexus. Raman spectra were recorded using a confocal Raman microscope (DXR, Thermo-Fisher Scientific) with 633 nm excitation from an argon ion laser. X-ray absorption near edge structure (XANES) and Extended X-ray absorption fine structure (EXAFS) experiments were performed on the XAFCA beamline of Singapore Synchrotron Light Source.

#### **1.4 Computational details**

All simulations on metal-organic frameworks were based on density functional theory (DFT) and carried out by using the projector augmented wave method (PAW) as implemented in the Vienna *ab initio* simulation package (VASP). The exchange and correlation functional was treated as generalized gradient approximation (GGA) of the Perdew-Burke-Ernzerhof (PBE) formula. The wave functions were expanded by using the plane waves up to a kinetic energy cutoff of 500 eV. Brillouin-zone integrations were approximated by using special  $k$ -point sampling of Monkhorst-Pack scheme with a  $k$ -point mesh resolution of  $2\pi * 0.03 \text{ \AA}^{-1}$ . The unit cell lattice vectors (unit cell shape and size) and atomic coordinates were fully relaxed until the force on each atom was less than  $0.02 \text{ eV \AA}^{-1}$ .

## 1.5 Electrochemical measurements

Electrochemical measurements were conducted on a CHI 760D electrochemical workstation using a three-electrode system. Glassy carbon (GC) electrode with a diameter of 5 mm was served as the working electrode. The catalyst ink was prepared by dispersing 5 mg of catalyst into 1 mL of mixed solution consisting of 50  $\mu\text{L}$  of 5 wt% Nafion, 800  $\mu\text{L}$  of isopropanol and 150  $\mu\text{L}$  of deionized water. Then the catalyst was loaded on the GC electrode by drop-casting 10  $\mu\text{L}$  of ink to reach a loading of 0.255  $\text{mg cm}^{-2}$ . A platinum wire electrode and saturated calomel electrode (SCE) were used as counter and reference electrodes, respectively. All the electrochemical data were recorded in 1 M KOH (pH= 13.62) electrolytes and potentials were converted to a reversible hydrogen electrode (RHE) via the equation:  $E(\text{RHE}) = E(\text{SCE}) + (0.24 + 0.0592 \text{ pH})$ . Before evaluating the OER activity, catalysts were activated by 100 cyclic voltammetry (CV) cycles across the potential window of 1.2-1.8 V vs. RHE at a scan rate of 50  $\text{mV s}^{-1}$ . Following the pre-activation process, linear sweep voltammetry (LSV) was performed at a scan rate of 5  $\text{mV s}^{-1}$ .  $iR$  drop was corrected using the uncompensated series resistance collected from electrochemical impedance spectroscopy (EIS) at a potential of 0.55 V vs. SCE with frequency from 1 to  $10^5$  Hz. The long-term stability tests were measured by chronopotentiometry at the current density of 10  $\text{mA cm}^{-2}$ .

## 1.6 Electrochemical active surface area (ECSA)

The electrochemically active surface area (ECSA) was determined by the double layer capacitance ( $C_{dl}$ ). To obtain the  $C_{dl}$  value, CV measurements were performed in non-Faradaic region at different scan rates of 4, 8, 12, 16, 20, 40, 60, 80 and 100  $\text{mV s}^{-1}$  (Figure S7).  $C_{dl}$  was

estimated by plotting the  $\Delta J = (J_a - J_c)/2$  against the scan rate. The linear slope is equivalent to the  $C_{dl}$ .

The  $C_{dl}$  can be further converted into ECSA using the specific capacitance value for a standard with  $1 \text{ cm}^{-2}$  of real surface area. The specific capacitance for a flat surface is normally between  $0.02\text{-}0.06 \text{ mF cm}^{-2}$ . GC electrode was used as the support, and the specific capacitance of GC can be regarded as the standard ( $178.92 \text{ }\mu\text{F cm}^{-2}$ ) in the following calculation.

The ECSA of each catalyst can be calculated according to:

$$A_{ECSA} = \frac{C_{dl} - \text{catalyst (mF cm}^{-2}\text{)}}{C_{dl} - \text{GC electrode (mF cm}^{-2}\text{) per ECSA cm}^{-2}}$$

Taking  $\text{IrO}_2$  as an example, upon the oxygen evolution reaction (OER), the  $\text{IrO}_2$  can be calculated as:

$$A_{ECSA} = \frac{56.52 \text{ (mF cm}^{-2}\text{)}}{178.92 \text{ (\muF cm}^{-2}\text{) per ECSA cm}^{-2}} = 315.90 \text{ cm}^2_{ECSA}$$

### 1.7 Faradaic efficiency calculation

The Faradaic efficiency was calculated as follows:

$$Fr = \left| \frac{I_r n_d}{I_d n_r N_{CL}} \right|$$

where  $I_r$  is the ring current,  $I_d$ , is the disk current,  $n_d$  and  $n_r$  are the electron transfer number of the reaction on disk ( $4\text{OH}^- \rightarrow 4\text{e}^- + 2\text{H}_2\text{O} + \text{O}_2$ ) and ring ( $2\text{H}_2\text{O} + \text{O}_2 + 2\text{e}^- \rightarrow 2\text{OH}^- + \text{H}_2\text{O}_2$ ), respectively. Moreover, the  $N_{CL}$  is the collect efficiency. ( $N_{CL} = 0.37$ )

### 1.8 Turnover frequency (TOF) calculation

The TOF values are calculated via the following equation:

$$\text{TOF} = \frac{|j|A}{mFn}$$

where  $|j|$  is the current density at an overpotential of 330 mV during the LSV measurement in 1.0 M solution.  $A$  stands for the area of the electrode ( $0.196 \text{ cm}^2$ ) and  $F$  is the Faradaic constant ( $96485 \text{ C mol}^{-1}$ ).  $m$  accounts for the electrons consumed to form one  $\text{H}_2$  or  $\text{O}_2$  molecule from water (2 electrons for hydrogen evolution reaction and 4 electrons for oxygen evolution reaction).  $n$  represents the quantity of active sites, and  $n$  can be calculated in two ways as follows.

If assuming all the metal ions take part in the electrocatalytic reaction, the value of  $n$  can be calculated based on the ICP results:

$$n = \frac{\frac{m_{\text{catalyst}} \times C_{\text{wt}\%-\text{Fe}}}{M_{\text{Fe}}} + \frac{m_{\text{catalyst}} \times C_{\text{wt}\%-\text{Ni}}}{M_{\text{Ni}}}}{A_{\text{electrode}}}$$

where  $m_{\text{catalyst}}$  is the catalyst loading on the disk electrode (0.05 mg),  $C_{\text{wt}\%}$  is the concentration of metal derived from ICP, and  $A_{\text{electrode}}$  is the area of disk electrode ( $0.196 \text{ cm}^2$ ). The calculated  $n$  is as follows.

The value of  $n$  can also be calculated by testing CV at  $50 \text{ mV s}^{-1}$  ranging from -0.2 to 0.6 V vs. RHE in phosphate buffered saline solution (PBS, pH = 7.0). The PBS solution is prepared by mixing up 38 mL of 0.2 M  $\text{NaH}_2\text{PO}_4$  solution and 62 mL of 0.2 M  $\text{Na}_2\text{HPO}_4$ . The quantity of active sites is calculated according to the following formula (Figure S6; *Nano Energy* 2018, 51, 26–36):

$$n = \frac{Q}{2F} = \frac{i \cdot t}{2F} = \frac{i \cdot V/u}{2F}$$

where Q is the cyclic voltammetric capacity obtained by integrating CV curves, F is the Faradaic constant (96485 C mol<sup>-1</sup>), i is the current density (A m<sup>-2</sup>), V is the voltage (v) and u is the scanning rate (V s<sup>-1</sup>).

**Table S1.** The value of n based on ICP and CV results, respectively, and the TOF calculated based on the CV derived value of n.

Sample	n (10 <sup>-5</sup> mmol cm <sup>-2</sup> ) based on ICP results	n (10 <sup>-5</sup> mmol cm <sup>-2</sup> ) based on CV results	TOF calculated from n based on CV results (s <sup>-1</sup> )
Fe-BDC	110	3.41	0.09
Fe <sub>2</sub> Ni <sub>1</sub> -BDC	100	2.04	6.06
Fe <sub>1</sub> Ni <sub>1</sub> -BDC	110	3.54	5.68
Fe <sub>1</sub> Ni <sub>2</sub> -BDC	110	3.68	11.53
Fe <sub>1</sub> Ni <sub>4</sub> -BDC	120	5.07	4.46
IrO <sub>2</sub>	9750	19.85	0.09

## 2. Supplemental Figures and Tables

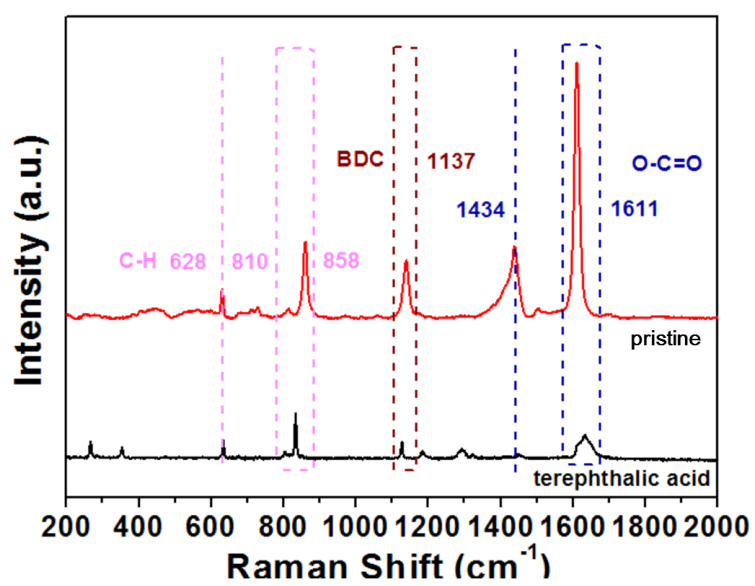


**Figure S1.** Raman spectra of Fe<sub>1</sub>Ni<sub>2</sub>-BDC and terephthalic acid.

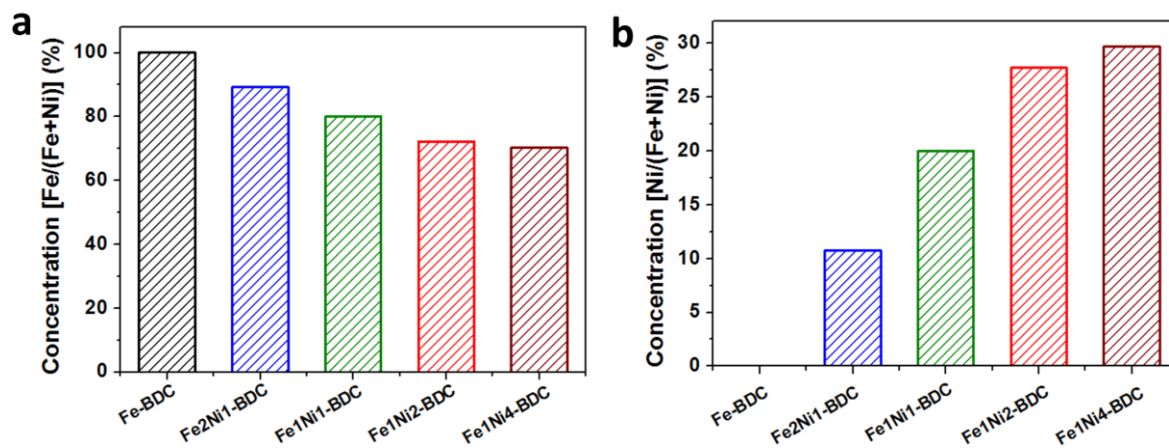


**Figure S2.** ICP analysis of Fe-BDC, Fe2Ni1-BDC, Fe1Ni1-BDC, Fe1Ni2-BDC and Fe1Ni4-BDC: (a) concentration of Fe, calculated by  $\text{Fe}/(\text{Fe}+\text{Ni})$ ; (b) concentration of Ni, calculated by  $\text{Ni}/(\text{Fe}+\text{Ni})$ .

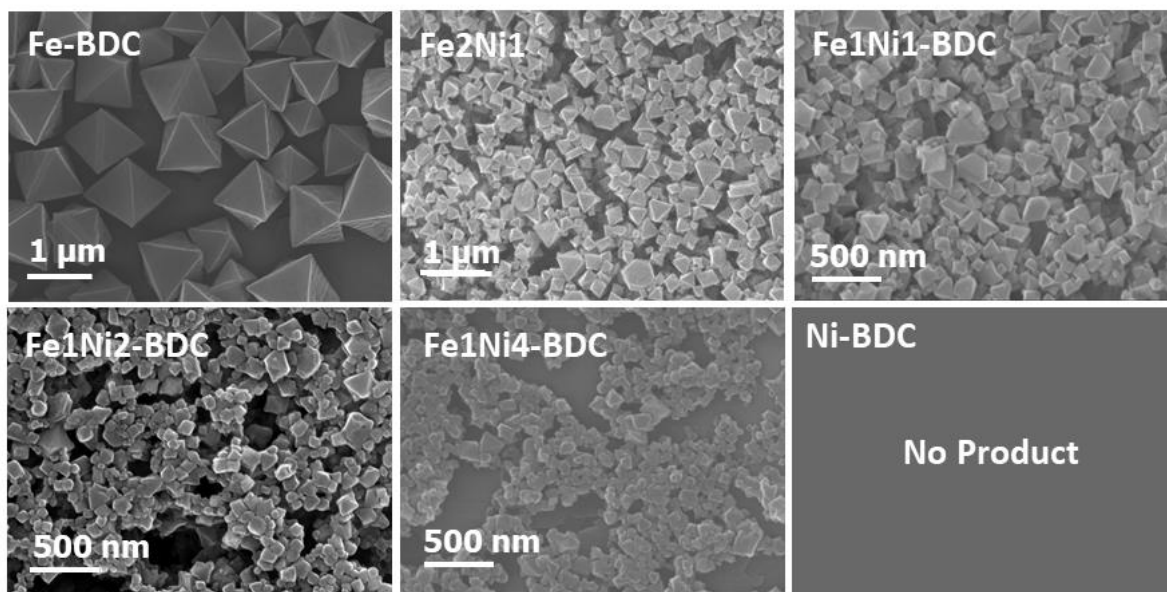


**Figure S3.** SEM images of Fe-BDC, Fe<sub>2</sub>Ni<sub>1</sub>-BDC, Fe<sub>1</sub>Ni<sub>1</sub>-BDC, Fe<sub>1</sub>Ni<sub>2</sub>-BDC and Fe<sub>1</sub>Ni<sub>4</sub>-BDC. The Ni-BDC cannot be achieved under the condition applied in the manuscript.

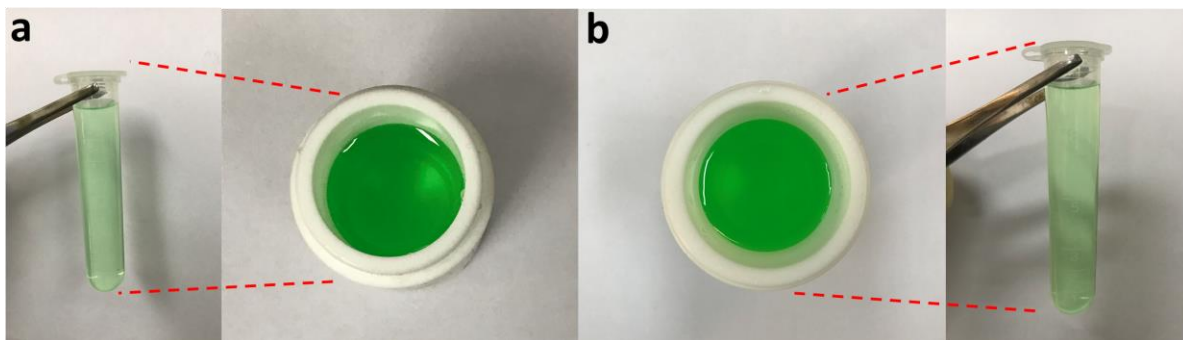


**Figure S4.** Images of before (a) and after (b) solvothermal process of Ni-BDC.

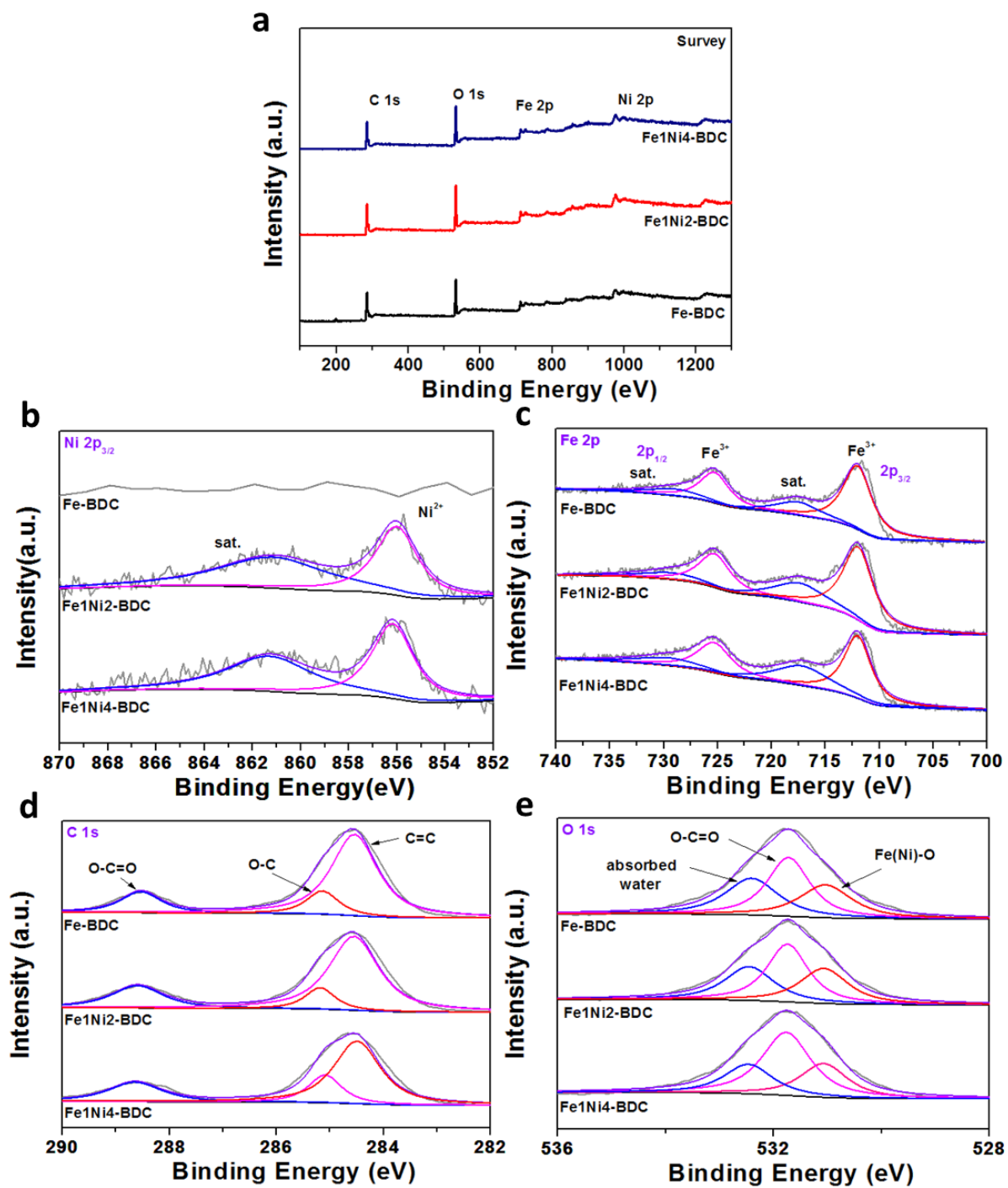


**Figure S5.** XPS characterization of Fe-BDC, Fe1Ni2-BDC and Fe1Ni4-BDC: (a) survey, (b) Ni 2p, (c) Fe 2p, (d) C 1s and (e) O 1s spectra.

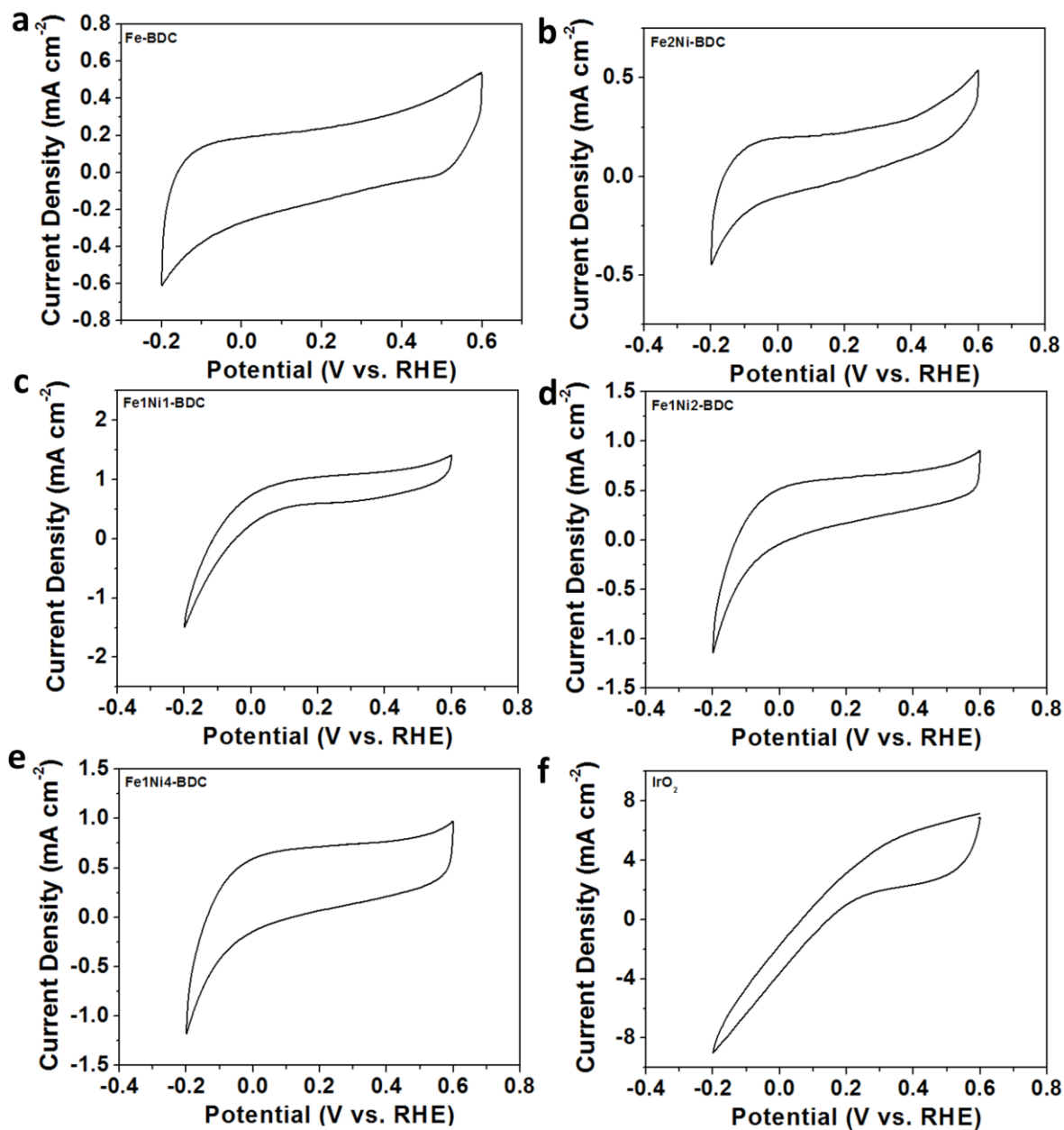


**Figure S6.** CV curves of (a) Fe-BDC, (b) Fe<sub>2</sub>Ni<sub>1</sub>-BDC, (c) Fe<sub>1</sub>Ni<sub>1</sub>-BDC, (d) Fe<sub>1</sub>Ni<sub>2</sub>-BDC, (e) Fe<sub>1</sub>Ni<sub>4</sub>-BDC and (f) IrO<sub>2</sub> in PBS solution (pH = 7.0) at a scan rate of 50 mV s<sup>-1</sup>.

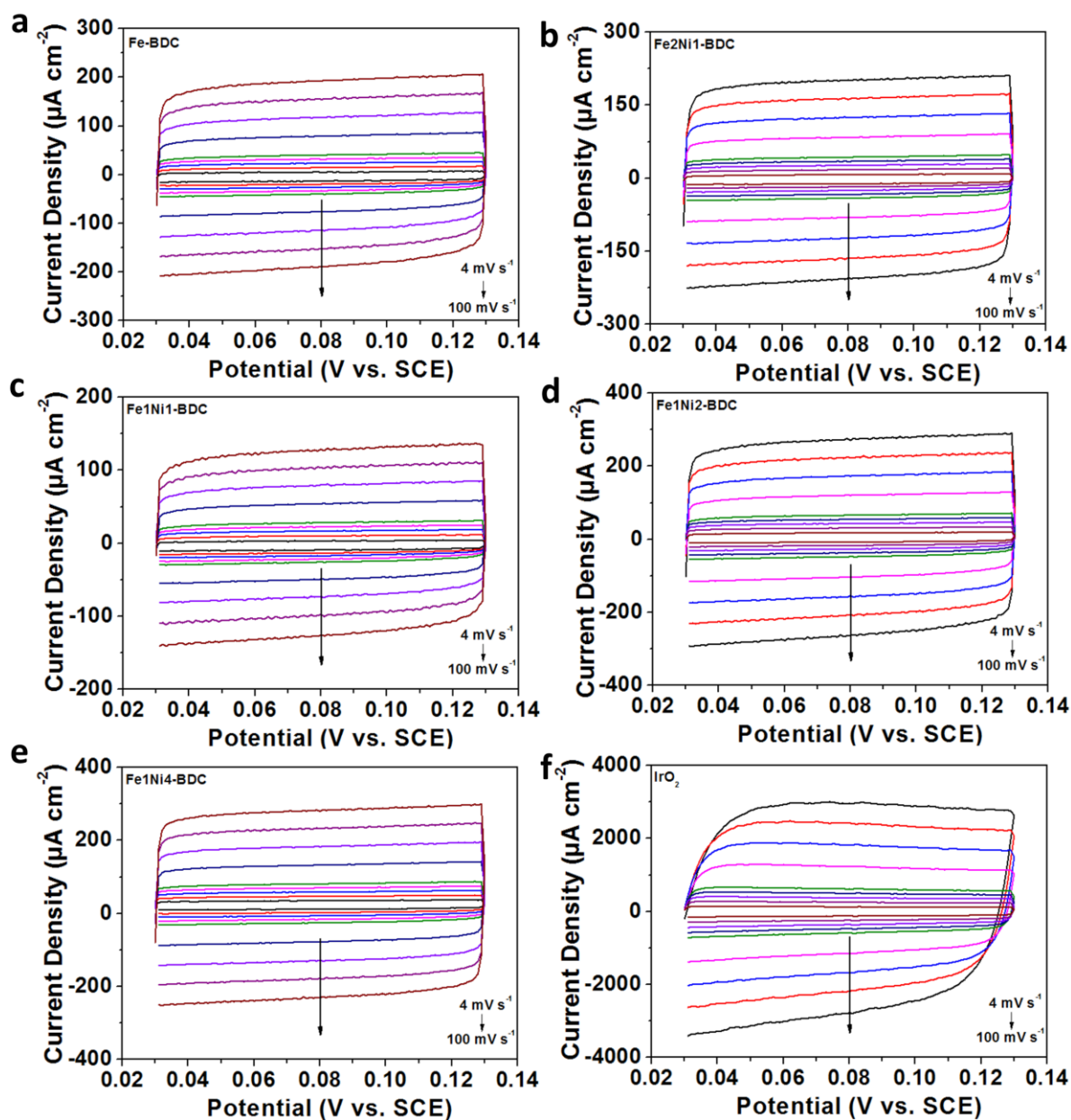


**Figure S7.** CV curves of (a) Fe-BDC, (b) Fe2Ni1-BDC, (c) Fe1Ni1-BDC, (d) Fe1Ni2-BDC, (e) Fe1Ni4-BDC and (f) IrO<sub>2</sub> at different scan rates from 4 to 100  $\text{mV s}^{-1}$ .

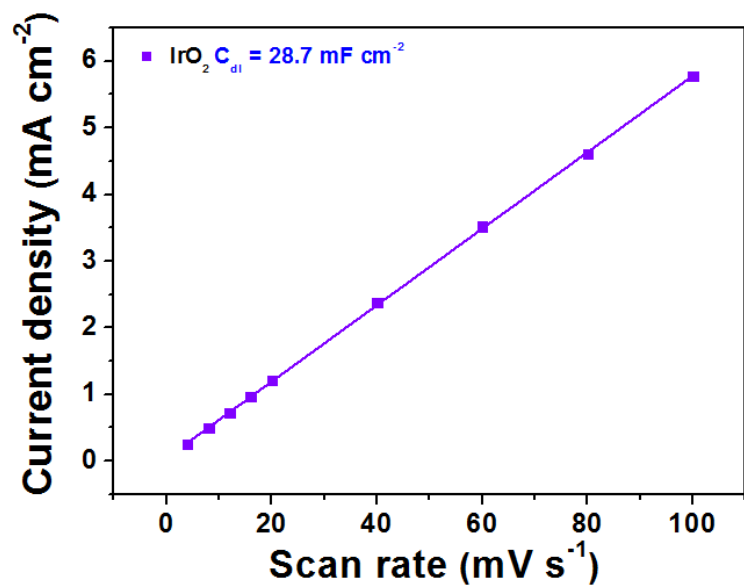


**Figure S8.** CV current density versus scan rate of IrO<sub>2</sub>, the linear slope is equivalent to the double-layer capacitance (C<sub>dl</sub>).

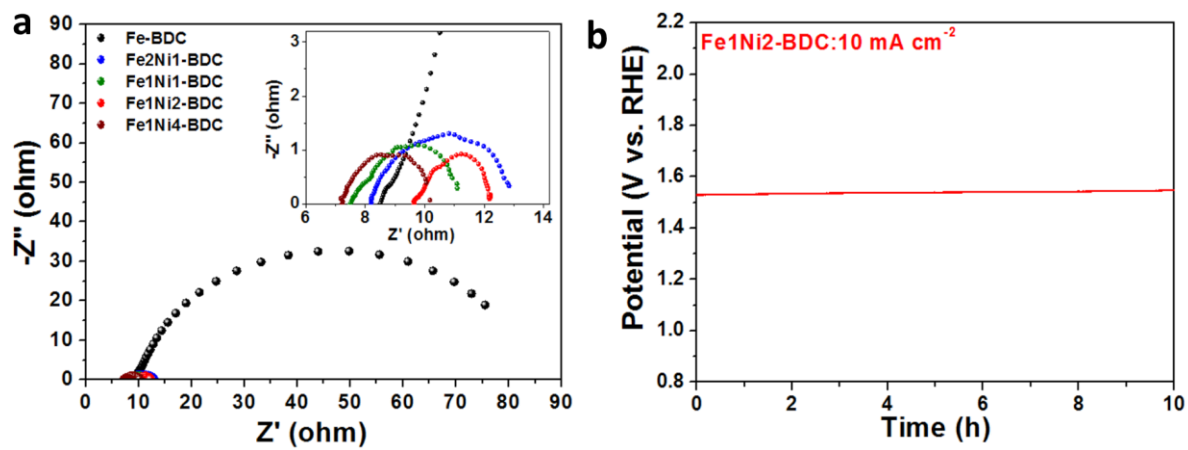


**Figure S9.** (a) The corresponding Nyquist plots of different catalysts, the inset shows enlargement of them. (b) Durability tests of Fe1Ni2-BDC in 1 M KOH at a constant current density of  $10 \text{ mA cm}^{-2}$ .

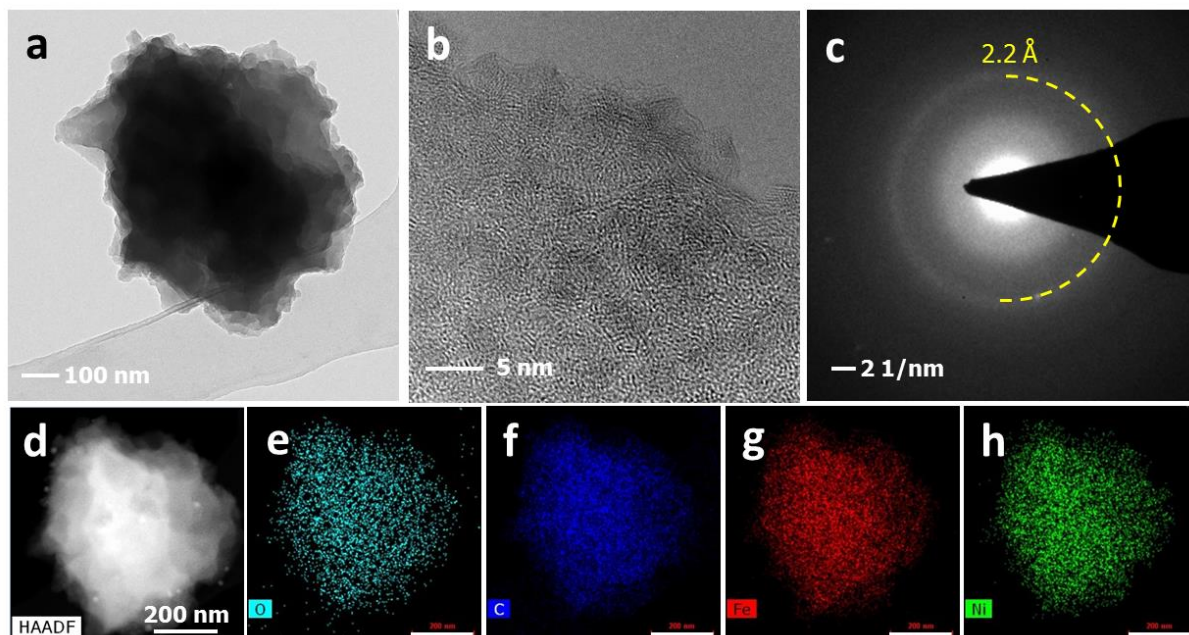


**Figure S10.** (a) TEM image, (b) HRTEM image and (c) SAED pattern, (d) HAADF-STEM image and (e-h) the corresponding EDX elemental maps of the Fe<sub>1</sub>Ni<sub>2</sub>-BDC after OER durability test in 1 M KOH for 2 h. Scale bar dimensions in e-h are all 200 nm.

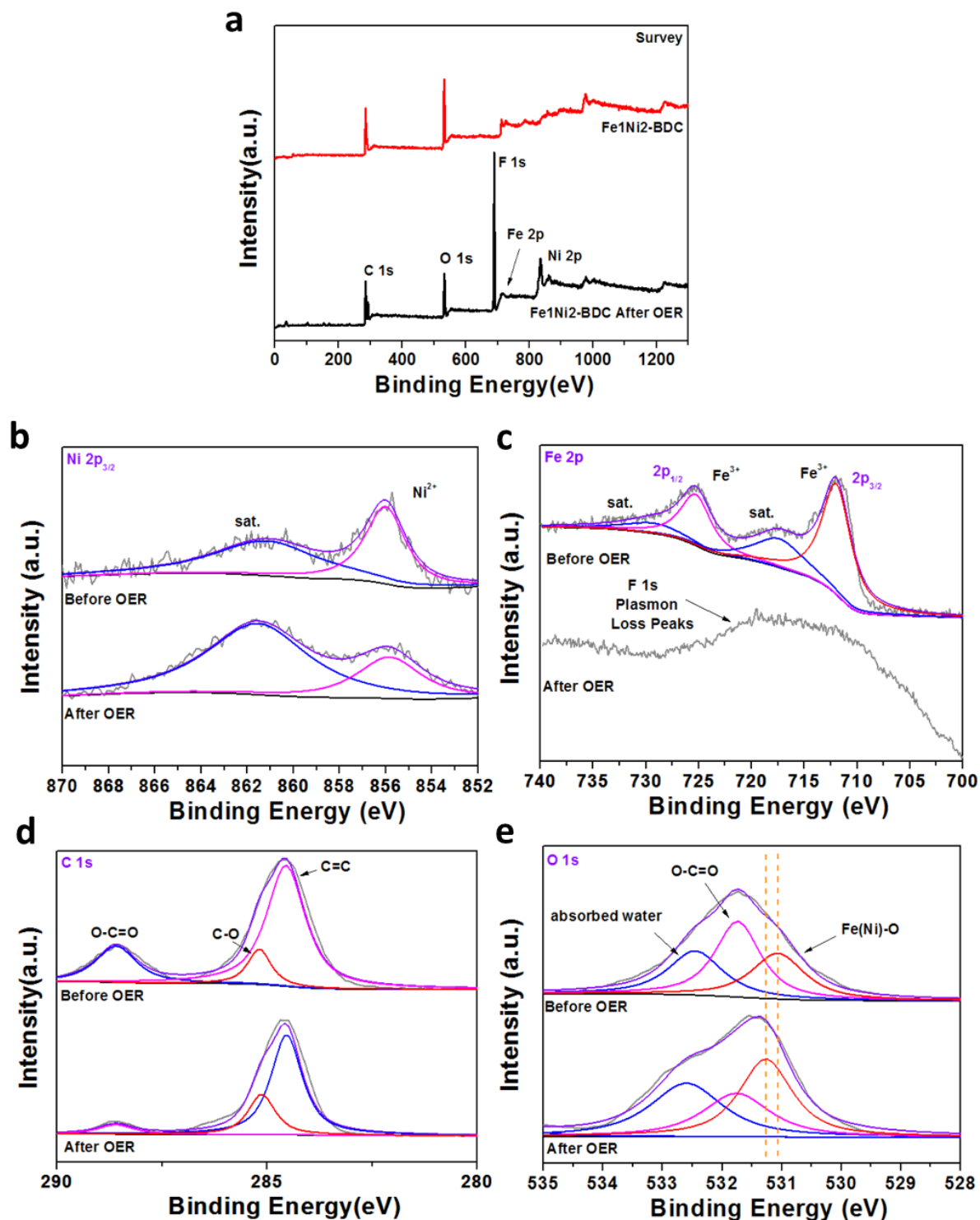


**Figure S11.** XPS characterization of Fe1Ni2-BDC and corresponding catalysts after 2 h durability test in 1 M KOH: (a) survey, (b) Ni 2p, (c) Fe 1s, (d) C 1s and (e) O 1s XPS spectra.

**Table S2.** Fitting parameters of Fe K-edge and Ni K-edge EXAFS curves.

sample	path name	N	R /Å	$\sigma^2$ /Å <sup>2</sup>	$\Delta E_0$ /eV	R factor / %
Fe-BDC <sup>a</sup>	Fe-O	6	1.988 (+/-0.006)	0.0073 (+/-0.0007)	-1.96 (+/-1.84)	0.0075
Fe1Ni2-BDC <sup>a</sup>	Fe-O	6	2.021 (+/-0.008)	0.0073 (+/-0.0010)	2.01 (+/-2.46)	0.0155
Fe1Ni2-BDC <sup>b</sup>	Ni-O	6	2.054 (+/-0.021)	0.0041 (+/-0.0010)	-0.57 (+/-3.28)	0.0181

N, R,  $\sigma^2$ ,  $\Delta E_0$  and R factor represent coordination number, distance between absorber and backscatter atoms, Debye-Waller factor to account for both thermal and structural disorders, inner potential correction and the goodness of the fit, respectively. <sup>a</sup>Fitting range:  $1.0 \leq R$  (Å)  $\leq 2.0$ ; <sup>b</sup>Fitting range:  $1.0 \leq R$  (Å)  $\leq 2.3$ . The results were fitted with N fixed.

**Table S3.** The OER performance of the as-synthesized  $\text{Fe}_x\text{Ni}_y\text{-BDC}$  samples and  $\text{IrO}_2$ .

Sample	Onset / mV	Overpotential / mV at 10 mA cm <sup>-2</sup>	Tafel slope / mV dec <sup>-1</sup>	TOF / s <sup>-1</sup> at 330 mV
Fe-BDC	278	419	76	0.02
Fe2Ni1-BDC	218	280	41	0.11
Fe1Ni1-BDC	220	281	36	0.17
Fe1Ni2-BDC	200	260	35	0.36
Fe1Ni4-BDC	219	280	42	0.16
$\text{IrO}_2$	241	340	66	0.02

**Table S4.** Comparisons of OER performance for various Fe/Ni-based and MOFs-based electrocatalysts tested in KOH.

Catalysts	$\eta$ / mV at 10 mA cm <sup>-2</sup>	Tafel slope / mV dec <sup>-1</sup>	References
<sup>a</sup> Fe1Ni2-BDC	260	42	this work
<sup>a</sup> Ni-Fe LDH hollow nanoprisms	280	49	<i>Angew Chem Int Ed</i> 2017, 130, 178
<sup>a</sup> LaSr <sub>3</sub> Co <sub>1.5</sub> Fe <sub>1.5</sub> O <sub>10-δ</sub>	388	84	<i>Nano Energy</i> 2017, 40, 115
<sup>a</sup> A <sub>2.7</sub> B-MOF-FeCo <sub>1.6</sub>	288	39	<i>Adv Energy Mater</i> 2018, 8(29), 1801564
<sup>a</sup> CoOx-ZIF/C	318	70	<i>Adv Funct Mater</i> 2017, 27, 1702546
<sup>a</sup> NiFe LDH	399	/	<i>Nano Energy</i> 2017, 39, 85
<sup>b</sup> NiFe-LDH/Co,N-CNF	312	/	<i>Adv Energy Mater</i> 2017, 7, 1700467
<sup>a</sup> Fe/Ni <sub>2.4</sub> /Co <sub>0.4</sub> -MIL-53	270	89	<i>Adv Mater</i> 2017, 29, 1700017
<sup>b</sup> Fe <sub>3</sub> -Co <sub>2</sub> @GC	283	43	<i>J Am Chem Soc</i> 2017, 139, 1778
<sup>b</sup> hollow Co <sub>3</sub> O <sub>4</sub> microtubes	290	84	<i>Angew Chem Int Ed</i> 2016, 56, 1324
<sup>b</sup> Ti <sub>3</sub> C <sub>2</sub> T <sub>x</sub> -CoBDC	410	48.2	<i>ACS Nano</i> 2017, 11, 5800
<sup>a</sup> CoO-MoO <sub>2</sub> nanocages	312	69	<i>Adv Funct Mater</i> 2017, 27, 1702324
<sup>a</sup> NiCoFe-MOF	320	49	<i>Adv Funct Mater</i> 2018, 28, 1802129

<sup>a</sup> Co/Co <sub>3</sub> O <sub>4</sub> @PGS	350	76	<i>Adv Energy Mater</i> 2018, 8, 1702900
<sup>a</sup> Ni <sub>0.6</sub> Co <sub>1.4</sub> P	300	80	<i>Adv Funct Mater</i> 2018, 28, 1706008
<sup>a</sup> Co <sub>3</sub> S <sub>4</sub> @MoS <sub>2</sub>	280	43	<i>Nano Energy</i> 2018, 47, 494
<sup>a</sup> 2D FeSe <sub>2</sub>	330	48	<i>Nano Energy</i> 2017, 31, 90
<sup>a</sup> P doped Co <sub>3</sub> O <sub>4</sub>	280	52	<i>Energy Environ Sci</i> 2017, 10, 2563
<sup>a</sup> NiCoP/C nanoboxes	330	96	<i>Angew Chem Int Ed</i> 2017, 129, 3955
<sup>a</sup> Multishelled Ni <sub>2</sub> P Hollow Microspheres	270	40	<i>Chem Mater</i> 2017, 29, 8539
<sup>a</sup> Mn-Fe phosphide nanorods	440	39	<i>Chem Mater</i> 2017, 29, 3048
<sup>b</sup> Co <sub>6.8</sub> Ni <sub>1.2</sub> W <sub>12</sub> O <sub>42</sub> (OH) <sub>4</sub> (H <sub>2</sub> O) <sub>8</sub> /NF	360	126	<i>Angew Chem Int Ed</i> 2017, 56, 4941
<sup>b</sup> PrBa <sub>0.5</sub> Sr <sub>0.5</sub> Co <sub>1.5</sub> Fe <sub>0.5</sub> O <sub>5</sub>	358	52	<i>Nat Commun</i> 2017, 8, 14586
<sup>b</sup> FeMnP/NF	280	57	<i>Nano Energy</i> 2017, 39, 444

---

Note. a and b indicate that the electrolyte is 1.0 M KOH and 0.1 M KOH, respectively.